



Investigation on $\text{Sr}_{0.2}\text{Na}_{0.8}\text{Nb}_{1-x}\text{V}_x\text{O}_3$ ($x=0.1, 0.2, 0.3$) as new ceramic anode materials for low-temperature solid oxide fuel cells



Ke-Ji Pan, A. Mohammed Hussain, Eric D. Wachsman*

University of Maryland Energy Research Center, University of Maryland, College Park, MD 20742, USA

HIGHLIGHTS

- Sr and V co-doped NaNbO_3 (SNNV) based alternative ceramic anode for low-temperature SOFCs.
- High conductivity of $300 \text{ S} \times \text{cm}^{-1}$ achieved at 450°C in H_2 .
- A ceramic anode compatible with GDC electrolyte.
- Ceramic anode with intrinsic catalytic activity for H_2 and CH_4 oxidation above 600°C .
- Peak power density of 280 mW/cm^2 achieved at 650°C in dry H_2 with Ni-GDC infiltration.

ARTICLE INFO

Article history:

Received 8 November 2016

Received in revised form

1 February 2017

Accepted 9 February 2017

Keywords:

Low-temperature solid oxide fuel cells (LT-SOFC)

Ceramic anode

High conductivity

Dry methane

Infiltration

ABSTRACT

Variants of SNNV ($\text{Sr}_{0.2}\text{Na}_{0.8}\text{Nb}_{1-x}\text{V}_x\text{O}_3$, $X = 0.1-0.3$) ceramic oxides were synthesized via wet chemical method. SNNVs show high electronic conductivity of $>100 \text{ S/cm}$ when reduced in hydrogen at a relatively low temperature of 650°C . In particular, 30% V-doped SNNV exhibited the highest conductivity of 300 S/cm at 450°C . In order to investigate the fuel cell performance, $\text{Gd}_{0.1}\text{Ce}_{0.9}\text{O}_{2-\delta}$ (GDC) based electrolyte-supported fuel cells were prepared to study the anode characteristics. $\text{Sr}_{0.2}\text{Na}_{0.8}\text{Nb}_{0.9}\text{V}_{0.1}\text{O}_3$ (SNNV10)-GDC composite was used as an anode and $\text{La}_{0.6}\text{Sr}_{0.4}\text{Co}_{0.2}\text{Fe}_{0.8}\text{O}_{3-\delta}$ (LSCF)-GDC as a cathode. Both electrodes were porous and sintered at 1050°C for 2 h in air. The anode side of the fuel cell was infiltrated with 10 wt% GDC/Ni-GDC precursor to activate the anode for fuel oxidation. I-V characteristics were determined in gas conditions such as dry/humidified hydrogen and methane at 650°C . With the infiltration Ni-GDC, peak power density (PPD) of 280 mW/cm^2 and 220 mW/cm^2 in dry H_2 and CH_4 , respectively, were obtained at 650°C , which is higher than GDC alone as infiltrate. The high resistances in the humidified conditions are attributed to the lower conductivity of SNNV10 in high P_{O_2} atmospheres.

© 2017 Elsevier B.V. All rights reserved.

1. Introduction

A Solid oxide fuel cell (SOFC) is an electrochemical device that converts chemical energy stored in fuels such as hydrogen or hydrocarbon into electrical power with high efficiency. SOFCs are all solid-state devices comprised of a dense gas tight electrolyte and a porous cathode and anode attached on either side of the electrolyte. Commonly used SOFC anode materials include Ni-YSZ and Ni-GDC cermets for high and low-temperature operations, respectively. Nickel based electrodes are catalytically active, however, they constitute major problems such as huge volume change upon redox cycling, carbon deposition in hydrocarbon fuels [1,2] and low

sulfur tolerance [3,4]. Highly electronic conductive ceramic anodes are considered to be an alternative for cermet anodes. Typical intermediate temperature-SOFC operates below 800°C and low-temperature SOFCs (LT-SOFC) operates $< 600^\circ\text{C}$. For low-temperature operation, it is critical to develop materials having high conductivity in that low-temperature range.

Several ceramic materials have been investigated as potential anodes for SOFCs [5–8]. Niobium-doped strontium titanate (SNT) had been explored as an anode material for SOFCs. SNT can achieve an electronic conductivity of 6.5 S cm^{-1} after reduction at 930°C with good redox stability [9]. However, SNT has to be reduced or sintered in H_2 at high temperature limiting their usage for intermediate or low-temperature SOFCs [10–12]. A low-temperature reduced SNT ($\text{Sr}_{0.875}\text{Ti}_{0.75}\text{Nb}_{0.25}\text{O}_3$) under 10% H_2/N_2 at 650°C over 24 h has shown a conductivity of only 0.2 S cm^{-1} , that further

* Corresponding author.

E-mail address: ewach@umd.edu (E.D. Wachsman).

proves this problem. Other potential materials, such as Mo-based double perovskites e.g., Sr_2MMoO_6 , and Ba_2MMoO_6 ($\text{M} = \text{Mn, Fe}$) should be prepared in reducing atmospheres to achieve high conductivities below 800 °C [13–22]. Most of the low-temperature electrolyte materials such like gadolinium-doped ceria and erbium-stabilized bismuth oxide should be fired in air to obtain a dense layer. Therefore, the half cell needs to be processed in air, which is not compatible with the anode fabrication. $\text{La}_{0.7}\text{Sr}_{0.3}\text{VO}_3$ (LSV) showed good conductivity ($\approx 100 \text{ S cm}^{-1}$) after reduction [23], but it undergoes a phase change during redox cycling, and volume expansion and shrinkage are considerably high when changed between air and reducing gas conditions making them less durable [23,24].

Strontium and vanadium co-doped sodium niobate (NaNbO_3) is a good ceramic material that can be prepared in air. At low-temperature (<650 °C) in reducing gas conditions, vanadium (V) is easily reduced to 4+ or even 3+ state and generates free electrons. Therefore, V-doped- NaNbO_3 can greatly improve the conductivity. Unlike LSV, V is the dopant in perovskite structure and the loss of lattice oxygen will not change the crystal structure. Higher valence cations such as Sr is doped at the A-site of the NaNbO_3 to stabilize the structure. In this work, the electrical conductivity of SNNV materials at various V-doping levels has been investigated. An electrolyte-supported SOFC was used to study the anode characteristics. The SOFC performance was analyzed both in dry and humidified gases such as H_2 and CH_4 .

2. Experimental

Based on their V-doping level, $\text{Sr}_{0.2}\text{Na}_{0.8}\text{Nb}_{0.9}\text{V}_{0.1}\text{O}_3$, $\text{Sr}_{0.2}\text{Na}_{0.8}\text{Nb}_{0.8}\text{V}_{0.2}\text{O}_3$ and $\text{Sr}_{0.2}\text{Na}_{0.8}\text{Nb}_{0.7}\text{V}_{0.3}\text{O}_3$ are called SNNV10, SNNV20, and SNNV30, respectively throughout this article. All compositions were synthesized through a modified glycine-nitrate method. A stoichiometric amount of strontium nitrate, sodium nitrate, niobium oxalate and ammonium metavanadate were dissolved in de-ionized water separately. The solutions were mixed slowly and glycine was added based on glycine to nitrate ratio 1:1. Citric acid was then added until the white precipitate disappears. The mixture was stirred and heated on a hot plate at 200 °C to evaporate the solvent until a viscous gel was formed. Ethanol was sprayed on the gel and manually ignited. After complete combustion, the residues of the reaction was collected and held at 400 °C for 2 h, and then calcined at 1000 °C for 4 h, at a ramp rate 3 °C/min. The calcined powders were ball milled in ethanol for 24 h and then sintered at 1300 °C for 4 h with a ramp rate of 3 °C/min.

To confirm phase purity, X-ray diffraction was performed on the sintered samples, using a Bruker D8 Advance diffractometer with $\text{CuK}\alpha$ radiation. The degree ranges from 20° to 80° with a step 0.015°/s. To examine the stability in reducing atmosphere, all samples were reduced and phase purity was determined.

To examine the possibility of reaction between the new anode and the electrolyte, SNNV30 was selected to confirm the chemical stability with YSZ and GDC. Same amount of calcined SNNV30 powder and GDC/YSZ were mixed, ball milled in ethanol for 24 h. The mixtures were dried in an oven and heated at 1300 °C for 4 h. The heated powder sample were analyzed using XRD to examine the phase purity.

Electronic conductivity was measured using four probe DC method. The SNNV powders were ball milled in ethanol for 24 h. Ethanol was dried and pellets were pressed using a hydraulic press. The green bodies were sintered at 1300 °C for 4 h and bar samples were used to determine the conductivity. Thin silver wires were attached to the bar and connected to a Keithley 2400 current source. The geometry factors were measured between the two voltage leads and the current source was used and set at 4 probe

mode. All SNNV samples were reduced in 10% H_2/N_2 at 650 °C for 24 h and the measurements were made in temperature ranges from 650 °C to 450 °C. The resistance values were monitored after providing sufficient time for stabilization.

SOFC performance was determined on GDC electrolyte-supported cells. A 260 μm thick GDC electrolyte was prepared by tape casting technique, following a standard lab procedure with Polyvinyl Butyral (PVB) as a binder, Butyl Benzyl Phthalate (BBP) as plasticizer and fish oil as a dispersant. The solvent system is ethanol-toluene mixture. The resulting tapes were dried and laminated to achieve desired thickness. The cells were punched from the green tape and sintered at 1450 °C for 4 h. SNNV10-GDC anode paste was prepared following a standard procedure. SNNV10 and GDC were mixed by the same weight. 12 μm and 1.8 μm Poly(methyl methacrylate) (PMMA) pore formers were added to the mixture to obtain a theoretical porosity of 50 vol%. The ESL vehicle (ElectroScience 441) was added to the mixtures to make a paste of screen printing consistency. The ink was then brush painted on the GDC electrolyte. The other side of the electrolyte was deposited with LSCF-GDC cathode using blade-coating technique. The electrode deposited assemblies were dried separately and co-fired at 1050 °C for 2 h.

To achieve high catalytic activity and ionic conductivity, nitrate precursor of Ni-GDC was infiltrated into the anode side. The nitrates were burned off by heat-treating the sample at 400 °C between each infiltration cycle. The Ni-GDC loading was determined by comparing the initial weight and final weight of the sample after infiltration. The final Ni-GDC loading was around 10 wt% with reference to the anode weight. The anode weight can be calculated based on the sample weight difference before and after applying the anode paste, because the ceramic powder content in the paste is known. The equation used to calculate anode weight is shown below.

$$\text{Anode Weight} = \delta \cdot (m_a - m_e) \quad (1)$$

δ = the weight ratio of ceramic powder in paste (41.9%)

m_e = weight of GDC electrolyte in grams

m_a = weight of GDC electrolyte and anode paste in grams

For comparison, GDC only infiltrated samples were prepared by the same method, and the GDC loading was around 10 wt%.

3. Results and discussion

SNNV compositions are single phases as shown in Fig. 1(a), however, few minor impurities at lower angle from 25 to 30° for higher V-doping levels were observed. This indicates that solubility limit of V in the perovskite phase is between 20 and 30%. The excess V can exist in V^{5+} oxidation state with small ionic radii (54 p.m., coordination number = 6) and high mobility. This can facilitate the easy formation of secondary phases such as NaVO_3 , $\text{Sr}_3\text{V}_2\text{O}_8$ and/or other unknown amorphous phases. The structural stability of SNNVs in the presence of H_2 as reducing gas was studied using XRD and the resulting pattern shown in Fig. 1(b). When V dopant level is below 20%, the phases are stable under reducing conditions.

The compositions SNNV10 and SNNV20 showed good structural stability even under H_2 -containing gas. Conductivity of n-type conductor is given by the relation,

$$\sigma = Z \cdot n \cdot \mu \quad (2)$$

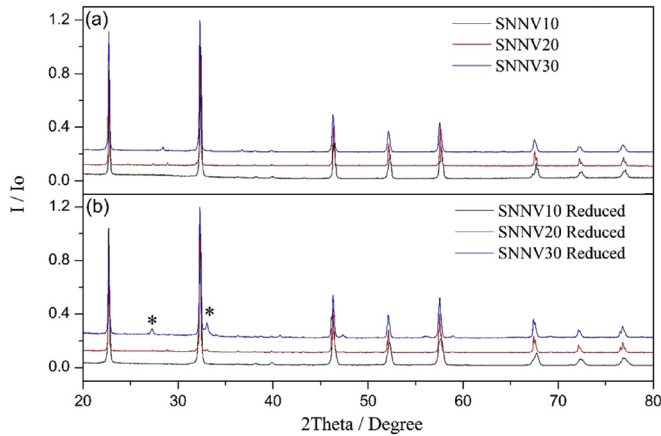


Fig. 1. (a) XRD Patterns of SNNV10, SNNV20 and SNNV30 after firing at 1300 °C for 4 h. All compositions have perovskite phases with minor impurities at low angles with high vanadium doped sample. (b) XRD patterns of reduced SNNV10, SNNV20 and SNNV30. SNNV10 and SNNV20 are still single phases. SNNV30 has impurities formed during reduction (* unknown impurities).

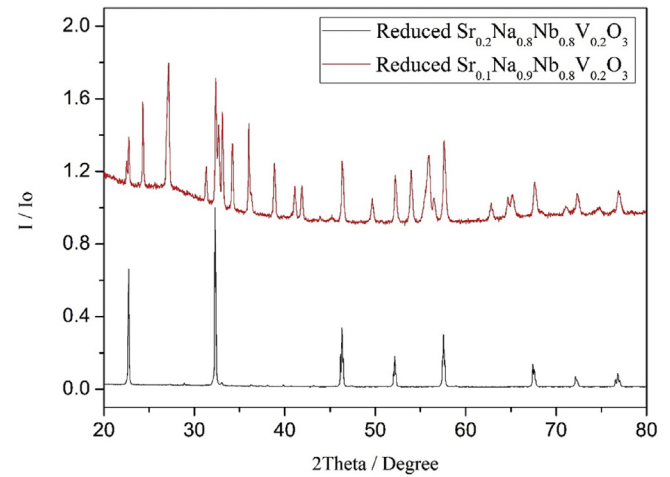


Fig. 2. Examples of different strontium doped SNNV samples. 20% strontium can stabilize the perovskite phase. 10% strontium doped sample totally decomposes after reduction.

where n is the concentration of charge carrier, Z is the electronic charge and μ is the charge carrier mobility.

In order to improve the electronic conductivity either the concentration or mobility of free electrons must be increased. At low P_{O_2} free electrons are generated, when lattice oxygen is taken away by reducing gas, such as H_2 , donating two free electrons and creating an oxygen vacancy as shown in Eq. (3).



When the crystalline lattice is easy to lose oxygen, the material is considered easily reducible, an Eq. (3) is likely to occur. The dopant V can easily change its valence state from $5+$ to $4+$ or even $3+$ under reducing conditions. Thus, doping V in $NaNbO_3$ can favor the removal of lattice oxygen, and increase the concentration of free electrons. However, it is to be noted that while oxygen removal improves the conductivity, it also has a negative effect. The resultant oxygen vacancies will compromise the materials stability, and potentially result in collapse of the lattice structure due to lower Coulombic force between cations and anions. In order to stabilize the perovskite structure, it is essential to dope a higher valence cation at the Na-site of the $NaNbO_3$ perovskite oxide to compensate this reduction in Coulombic force.

Sr was doped in the Na-site due their comparable ionic radii. (Sr 144pm, Na 136pm, coordination number = 12), and the XRD pattern of the resultant sample is shown in Fig. 2. It must be noted that 10% Sr in A-site is not stable in H_2 -containing atmosphere. However, the composition with 20% Sr at A-site is stable without decomposition, thus doping with appropriate amount of higher valence A-site cation can stabilize the lattice structure under reducing conditions.

After reduction at 650 °C in hydrogen, all SNNV samples show high conductivities and exhibit metallic behavior. The metallic type conduction is favorable for fabricating anode-supported LT-SOFCs and is shown in Fig. 3. At 450 °C, SNNV30 has the highest conductivity around $300 \text{ S} \times \text{cm}^{-1}$ and 10% V doped sample, SNNV10, has a conductivity of $130 \text{ S} \times \text{cm}^{-1}$, which is still high enough for anode support.

V-doped $NaNbO_3$ not only has high concentration of free electrons, it also has high electron mobility. According to electron hopping mechanism, electrons hop among multivalent B-Site cations. So in these compositions, the electron hopping routes can be

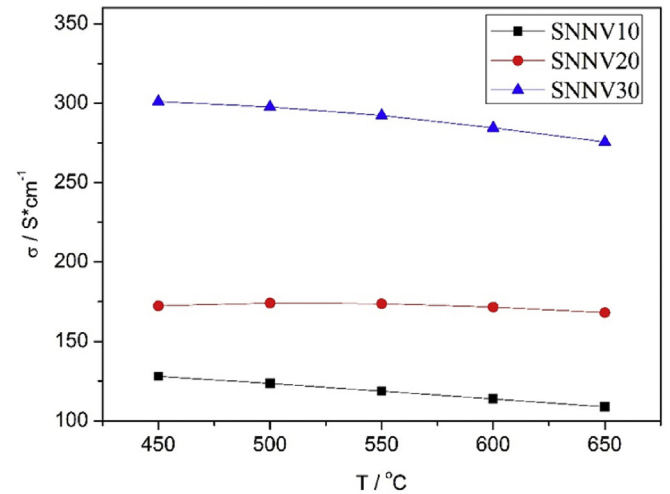


Fig. 3. Conductivities of SNNV10, SNNV20 and SNNV30 after reduction in 10% H_2 /90% N_2 .

as follows.



When B-site cations release free electrons, the valency decreases, and when the electron incorporates into B-site cations, the valency increases. If the B-site valency is easy to shift, it promotes a high electron mobility due to fast hopping process. Niobium and vanadium are all multivalent cations and the valence states can rapidly change. Therefore, perovskites with Nb and V as B-site cations have potential for high electronic conductivity [25,26].

Considering possible high mobility of V, it is essential to determine the reactivity between SNNVs and common electrolytes such as YSZ and GDC. SNNV30 was selected for compatibility tests because it has the highest tendency to react with electrolytes due to

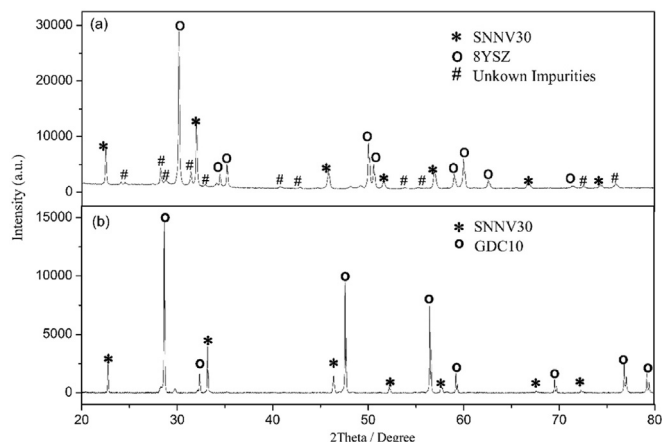


Fig. 4. (a) High temperature treated (1300 °C) nano 8YSZ and SNNV30 mixture. They react with each other and form unknown materials. (b) High temperature treated (1300 °C) nano GDC and SNNV30 mixture. No reaction between the two compounds.

high V content. XRD patterns in Fig. 4(a) show YSZ reacts with SNNV30 at high temperature and forms unknown phases. However, SNNV30 and GDC10 show their respective single phase up to 1300 °C in air as shown in Fig. 4(b). This indicates that compatibility between GDC and SNNV material is good without any unwanted reactions.

SNNV10 was selected for further analysis of anode performance, as it has sufficient conductivity ($130 \text{ S} \times \text{cm}^{-1}$) and with lower vanadium content would cause fewer fabrication issues due to vanadium diffusion. To improve the thermal mismatch between anode and the electrolyte, SNNV10-GDC composite was prepared as the anode. A 260 μm thick dense GDC electrolyte supported cell with both cathode and anode co-fired at 1050 °C was tested in dry/wet H_2 and dry/wet CH_4 . Initially SNNV10-GDC samples infiltrated with GDC were examined, and the cell performances are shown in Fig. 5(a). The purpose of infiltrating GDC is to cover the SNNV10 surface with ionic conductors to extend the triple phase boundary [27]. At 650 °C, the SOFC performance in hydrogen are 135 mW/cm^2 in wet and 180 mW/cm^2 in dry conditions. In other words, without

metallic catalyst, (such as Ni, Pd or Pt), SNNV10 can act as a catalyst for fuel oxidation. Therefore, we propose the possibility that SNNV10 has the capability to catalyze hydrogen or methane oxidation due to the variable valence state of V-cation.

It has been reported that V-containing compounds can be used as catalyst to partially oxidize hydrocarbons [28,29]. However, for CH_4 , the performance is much lower, around 40 mW/cm^2 in dry CH_4 and 35 mW/cm^2 in wet CH_4 . The catalytic activity is not high enough to accelerate methane oxidation reaction compared with hydrogen. Considering the low vanadium doping level in SNNV10, increasing vanadium dopant amount may improve hydrocarbon performance. Nevertheless, increasing V amount in the system should be carefully considered, as high V content may cause fabrication issues.

Moreover, in the humidified fuel, the cell outputs are lower both in hydrogen or methane as the feed, unlike typical Ni-YSZ or Ni-GDC. R. J. Gorte et al. also observed there was a performance drop for their sodium tungsten bronze infiltrated cell in humidified hydrogen [30]. The reduction in performance was attributed to an ohmic resistance increase for sodium tungsten bronze, when the cell is exposed to wet atmosphere. Considering SNNV10, it may be the same case as we also found there was an ohmic resistance increases shown in Fig. 5(b). The reduced performance in the presence of moisture could be due to higher P_{O_2} . As SNNV10 is an n-type conductor and at higher P_{O_2} the electronic conductivity is lower. It is also noted that an ohmic resistance of $0.48 \Omega \cdot \text{cm}^2$ at 650 °C was obtained for the SOFC tested in dry H_2 (Fig. 5(b)). This value is lower than the expected ohmic resistance based on the ionic conductivity of GDC electrolyte indicating possible partial reduction of Ce^{4+} or cation diffusion from anode to the electrolyte resulting in lowered ohmic resistance [31].

To improve the performance further, Ni-GDC precursor was infiltrated into the SNNV10-GDC instead of GDC. When Ni-GDC was infiltrated, the catalytic activities were enhanced both in dry H_2 and dry CH_4 as shown in Fig. 6. At 650 °C, the peak power density (PPD) in dry H_2 is 280 mW/cm^2 , 50% improvement compared with GDC only infiltrated sample. The PPD in CH_4 is 220 mW/cm^2 , 5 times higher than the no-nickel cell. At 600 °C, the cell generates 150 mW/cm^2 and 115 mW/cm^2 in H_2 and CH_4 , respectively. For a low temperature SOFC (<600 °C), the infiltration of catalyst is necessary, especially when hydrocarbons are used as fuel due to

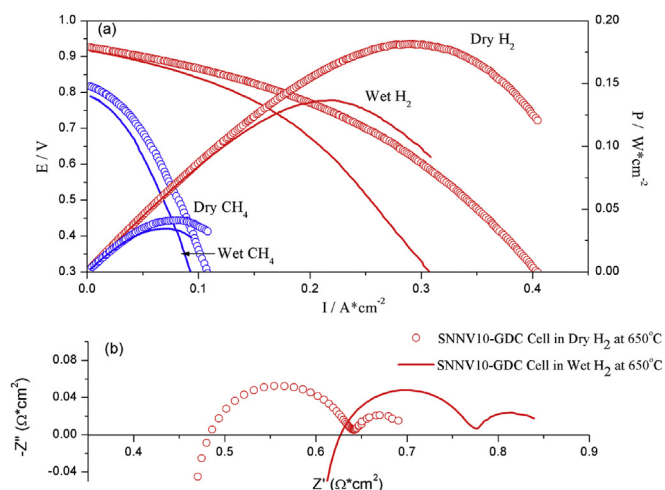


Fig. 5. (a) 260 μm GDC supported cell with SNNV10-GDC anode and LSCF-GDC cathode. 10 wt% GDC infiltrated into SNNV10-GDC anode. Cell was tested at 650 °C in H_2 and CH_4 . CH_4 performance is much lower than H_2 performance. In dry conditions the cell works better. (b) Impedance comparison between SNNV10-GDC cells in dry and humidified hydrogen at 650 °C. An ohmic resistance increase was observed when switching to humidified fuel.

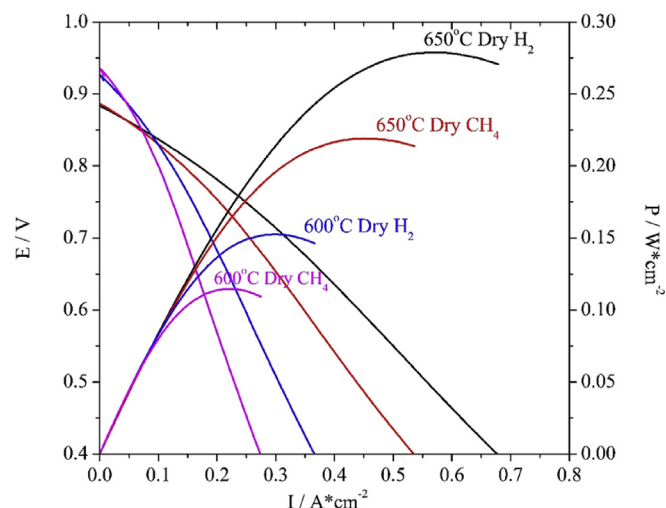


Fig. 6. 260 μm GDC supported cell with SNNV10-GDC anode and LSCF-GDC cathode. 10 wt% Ni-GDC infiltrated into SNNV10-GDC anode. Cell was tested in dry H_2 and dry CH_4 .

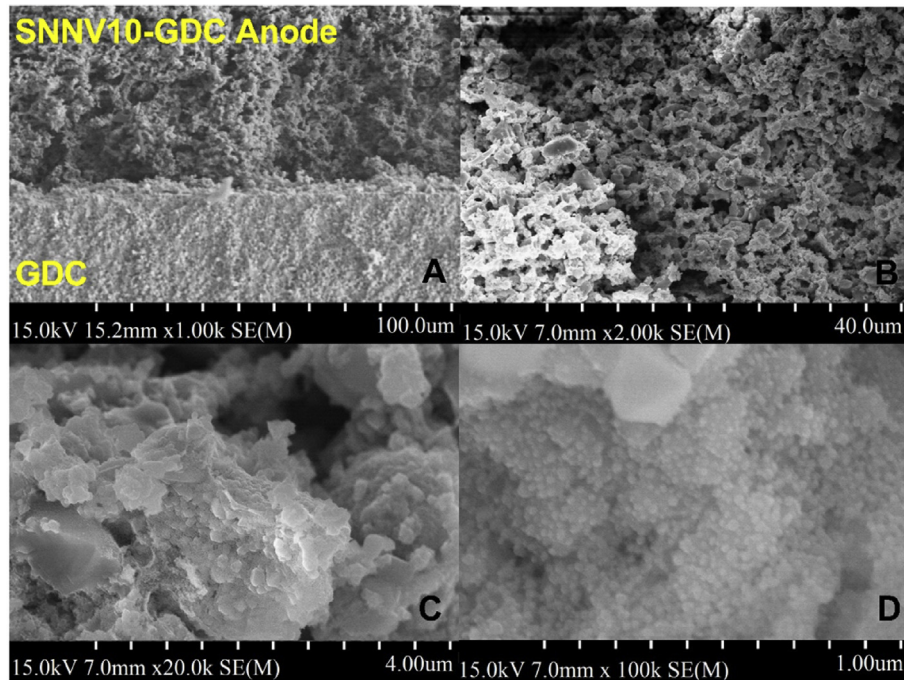


Fig. 7. SEM images of cell structure. (A) Fired SNNV10-GDC anode on top of GDC electrolyte (B) Anode microstructure. (C) Infiltrates on SNNV10-GDC backbone (D) well distributed Ni-GDC nano particles.

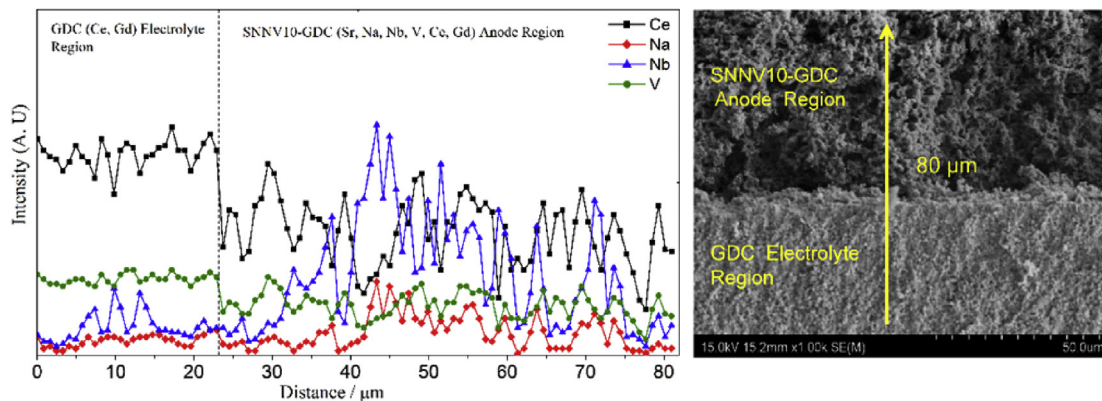


Fig. 8. EDS analysis of the interface between GDC electrolyte and SNNV10-GDC anode. No sodium and niobium diffusion but there is vanadium migrating from the anode to the electrolyte.

their lower reaction kinetics.

The cell cross section SEM is shown in Fig. 7(A–D). The pore morphology in the anode can dramatically affect infiltration efficiency. A homogeneous PMMA of 10 μm were initially used as pore formers, but there are a lot of closed pores and the connections between pores are easily blocked by infiltrates, which limits further infiltration resulting in lower loading. By mixing different PMMAs (12 μm and 5 μm), the microstructure illustrated a better pore percolation resulting in better infiltration and gas diffusion. In Fig. 7D, a well dispersed Ni-GDC nano particles are seen.

The EDS analysis in Fig. 8 shows the elemental distribution along the anode through the electrolyte. Because of low temperature firing (1050 °C), Na and Nb are still present only in the anode region implying no diffusion of such elements into the electrolyte region. However, V diffuses into the electrolyte due to its small ionic radii when compared to other elements in the anode. It is to be noted that such diffusion did not have any detrimental effect on the

Open Circuit Voltage (OCV) of the electrolyte supported-SOFCs.

4. Conclusion

Different compositions of SNNV were synthesized via wet chemical method and high conductivities were achieved at 650 °C. SNNV10 has a conductivity of $130 \text{ S} \cdot \text{cm}^{-1}$ and SNNV30 has $300 \text{ S} \cdot \text{cm}^{-1}$. Because of vanadium diffusion at high temperatures, it is preferred to fabricate the cell at relatively lower temperatures. After infiltrating Ni-GDC into the anode, the GDC electrolyte supported cell has PPDs of 280 mW/cm^2 and 220 mW/cm^2 in dry H_2 and dry CH_4 respectively at 650 °C. When the temperature is lowered to 600 °C, the PPDs are 150 mW/cm^2 and 115 mW/cm^2 in H_2 and CH_4 , respectively under dry conditions. Infiltration of GDC can extend the triple phase boundary and provide ionic conductivity. If there is no nickel as catalyst, the SNNV10 can intrinsically catalyze H_2 and has an appropriate output. As a result, with no

metal catalyst, this full ceramic SOFC can work efficiently in hydrogen, without any poisoning and redox cycling problems caused by a metal component. However, the full ceramic SOFC requires catalyst like Ni to perform well in methane, due to the relatively lower catalytic activity of SNNV10 than Ni metal. Unlike Ni-cermet anode, SNNV10 has lower performance in humidified conditions because of higher P_{O_2} , which decreases conductivity. We also observed vanadium diffusion, to prevent this, low temperature cell firing is needed to fabricate anode supported thin electrolyte cells.

Acknowledgements

We acknowledge the support of the DOE ARPA-E (DE-AR0000494), Redox Power Systems, LLC, and the University of Maryland.

References

- [1] J.-H. Koh, Y.-S. Yoo, J.-W. Park, H.C. Lim, Carbon deposition and cell performance of Ni-YSZ anode support SOFC with methane fuel, *Solid State Ionics* 149 (2002) 157–166.
- [2] J. Maček, B. Novosel, M. Marinšek, Ni-YSZ SOFC anodes—minimization of carbon deposition, *J. Eur. Ceram. Soc.* 27 (2007) 487–491.
- [3] Z. Cheng, M. Liu, Characterization of sulfur poisoning of Ni-YSZ anodes for solid oxide fuel cells using in situ Raman microspectroscopy, *Solid State Ionics* 178 (2007) 925–935.
- [4] Y. Matsuzaki, I. Yasuda, The poisoning effect of sulfur-containing impurity gas on a SOFC anode: Part I. Dependence on temperature, time, and impurity concentration, *Solid State Ionics* 132 (2000) 261–269.
- [5] Q. Fu, F. Tietz, Ceramic-based anode materials for improved redox cycling of solid oxide fuel cells, *Fuel Cells* 8 (2008) 283–293.
- [6] C. Graves, B.R. Sudireddy, M. Mogensen, Molybdate based ceramic negative-electrode materials for solid oxide cells, *ECS Trans.* 28 (2010) 173–192.
- [7] A. Atkinson, et al., Advanced anodes for high-temperature fuel cells, *Nat. Mater.* 3 (2004) 17–27.
- [8] X. Zhou, N. Yan, K.T. Chuang, J. Luo, Progress in La-doped SrTiO₃ (LST)-based anode materials for solid oxide fuel cells, *Rsc Adv.* 4 (2014) 118–131.
- [9] P.R. Slater, D.P. Fagg, J.T. Irvine, Synthesis and electrical characterisation of doped perovskite titanates as potential anode materials for solid oxide fuel cells, *J. Mater. Chem.* 7 (1997) 2495–2498.
- [10] A.M. Hussain, et al., Improved ceramic anodes for SOFCs with modified electrode/electrolyte interface, *J. Power Sources* 212 (2012) 247–253.
- [11] A.M. Hussain, J.V. Høgh, W. Zhang, N. Bonanos, Efficient ceramic anodes infiltrated with binary and ternary electrocatalysts for SOFCs operating at low temperatures, *J. Power Sources* 216 (2012) 308–313.
- [12] A.M. Hussain, J.V. Høgh, T. Jacobsen, N. Bonanos, Nickel-ceria infiltrated Nb-doped SrTiO₃ for low temperature SOFC anodes and analysis on gas diffusion impedance, *Int. J. hydrogen energy* 37 (2012) 4309–4318.
- [13] Y.-H. Huang, R.I. Dass, Z.-L. Xing, J.B. Goodenough, Double perovskites as anode materials for solid-oxide fuel cells, *Science* 312 (2006) 254–257.
- [14] R. Martinez-Coronado, J. Alonso, A. Aguadero, M. Fernandez-Diaz, Optimized energy conversion efficiency in solid-oxide fuel cells implementing SrMo_{1-x}Fe_xO_{3-δ} perovskites as anodes, *J. Power Sources* 208 (2012) 153–158.
- [15] T. Wei, Y. Ji, X. Meng, Y. Zhang, Sr₂NiMoO_{6-δ} as anode material for LaGaO₃-based solid oxide fuel cell, *Electrochem. Commun.* 10 (2008) 1369–1372.
- [16] P. Zhang, Y.-H. Huang, J.-G. Cheng, Z.-Q. Mao, J.B. Goodenough, Sr₂CoMoO₆ anode for solid oxide fuel cell running on H₂ and CH₄ fuels, *J. Power Sources* 196 (2011) 1738–1743.
- [17] A.B. Muñoz-García, M. Pavone, E.A. Carter, Effect of antisite defects on the formation of oxygen vacancies in Sr₂FeMoO₆: implications for ion and electron transport, *Chem. Mater.* 23 (2011) 4525–4536.
- [18] A. Markov, et al., Structural features, nonstoichiometry and high-temperature transport in SrFe_{1-x}Mo_xO_{3-δ}, *J. Solid State Chem.* 182 (2009) 799–806.
- [19] Y.-H. Huang, et al., Double-perovskite anode materials Sr₂MMoO₆ (M = Co, Ni) for solid oxide fuel cells, *Chem. Mater.* 21 (2009) 2319–2326.
- [20] Y.-H. Huang, R.I. Dass, J.C. Denyszyn, J.B. Goodenough, Synthesis and characterization of Sr₂MgMoO_{6-δ} an anode material for the solid oxide fuel cell, *J. Electrochem. Soc.* 153 (2006) A1266–A1272.
- [21] Q. Zhang, T. Wei, Y.-H. Huang, Electrochemical performance of double-perovskite Ba₂MMoO₆ (M = Fe, Co, Mn, Ni) anode materials for solid oxide fuel cells, *J. Power Sources* 198 (2012) 59–65.
- [22] L. Zhang, Q. Zhou, Q. He, T. He, Double-perovskites A₂FeMoO_{6-δ} (A = Ca, Sr, Ba) as anodes for solid oxide fuel cells, *J. Power Sources* 195 (2010) 6356–6366.
- [23] N.M. Vo, M.D. Gross, The effect of vanadium deficiency on the stability of Pd and Pt catalysts in lanthanum strontium vanadate solid oxide fuel cell anodes, *J. Electrochem. Soc.* 159 (2012) B641–B646.
- [24] M. Cooper, K. Channa, R. De Silva, D.J. Bayless, Comparison of LSV/YSZ and LSV/GDC SOFC anode performance in coal syngas containing H₂S, *J. Electrochem. Soc.* 157 (2010) B1713–B1718.
- [25] D. Oka, Y. Hirose, S. Nakao, T. Fukumura, T. Hasegawa, Intrinsic high electrical conductivity of stoichiometric SrNbO₃ epitaxial thin films, *Phys. Rev. B* 92 (2015) 205102.
- [26] J.A. Moyer, C. Eaton, R. Engel-Herbert, Highly conductive SrVO₃ as a bottom electrode for functional perovskite oxides, *Adv. Mater.* 25 (2013) 3578–3582.
- [27] A.M. Hussain, et al., Effective improvement of interface modified strontium titanate based solid oxide fuel cell anodes by infiltration with nano-sized palladium and gadolinium-doped cerium oxide, *Electrochim. acta* 113 (2013) 635–643.
- [28] K. Stein, et al., The oxidation of hydrocarbons on simple oxide catalysts, *J. Air Pollut. Control Assoc.* 10 (1960) 275–281.
- [29] U.R. Pillai, E. Sahle-Demessie, Vanadium phosphorus oxide as an efficient catalyst for hydrocarbon oxidations using hydrogen peroxide, *New J. Chem.* 27 (2003) 525–528.
- [30] L. Adjianto, R. Küngas, J. Park, J.M. Vohs, R.J. Gorte, SOFC anodes based on infiltration of tungsten bronzes, *Int. J. Hydrogen Energy* 36 (2011) 15722–15730.
- [31] A.M. Hussain, K.-J. Pan, I.A. Robinson, T. Hays, E.D. Wachsman, Stannate-based ceramic oxide as anode materials for oxide-ion conducting low-temperature solid oxide fuel cells, *J. Electrochem. Soc.* 163 (2016) F1198–F1205.